State-space Modeling of Multi-mode-controlled Induction Motor Drive

Zhe Zhang[1], Muhammed Ali Gultekin[1], Ali M. Bazzi[1,2]
1. Department of Electrical and Computer Engineering, University of Connecticut, USA
2. Department of Electrical and Computer Engineering, American University of Beirut, Lebanon
{zhe.4.zhang, muhammed_ali.gultekin, bazzi}@uconn.edu

***Abstract*— The theory of switched systems which focuses on stability and control synthesis of systems with multiple modes or different dynamics, has gained significant attention from control theorists, computer scientists, and practicing engineers. Switching between motor controllers due to sensor faults, faster response, or targeted dynamics, open a new dimension of shaping a motor drive's performance. There are three main types of control strategies for induction motor drives: namely volts per hertz (V/f) control, field-oriented control (FOC), direct torque control (DTC). Multi-mode-controlled induction motor drive can be modelled as a switched system where each control mode results in different motor dynamics. In this paper, a comprehensive state-space model of an induction motor drive under different control mode is developed. Detailed analysis as well as simulation results are included to demonstrate the validity of the state-space representation for induction motor under different mode.**

Keywords—induction motor drive, switched system, switched control, state-space representation, multi-mode control.

I. INTRODUCTION

Induction motors (IMs) are widely used in electrical drives because of their ruggedness and relatively low cost. Scalar control, namely volts per hertz (V/f) control [1], offers the simplest solution in applications such as pumps, compressors, heating, ventilation, and air conditioning, where the transient performance of the motor is not of great concern. It also relies on no or minimal number of sensors. On the other hand, advanced control techniques such as indirect field-oriented control (IFOC) and direct torque control (DTC) have also been well-established for high-performance adjustable speed drives (ASDs). All three control modes can be integrated in one electrical drive due to the enhanced computing power of digital signal processors (DSPs), which will make the whole drive more robust and can withstand sensor failures, giving engineers and operators flexibility on shaping a drive's response.

A switched system has hybrid dynamic features. It consists of a finite number of subsystems described by discrete (or continuous) time dynamics and a switching rule governing the switching among them. A typical architecture of multi-controller switched system is shown in Fig. 1. A high-level decision maker (supervisor) determines which controller is to be connected in closed loop with the plant at each instant of time [5]. Fig. 2 illustrates the system architecture of an induction motor drive with three admissible modes. Since the induction motor (IM) drive exhibits different dynamics depending on the selected mode, it can be modeled as a switched system. Three subsystems are embedded within the switched system: V/f-controlled, IFOC-controlled, and DTC-controlled IM drive.

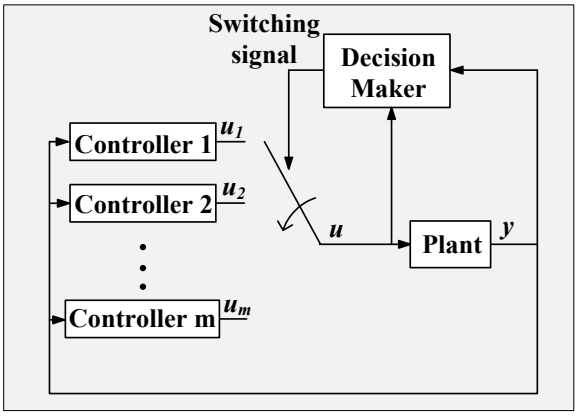

Fig. 1. A Multi-controller switched system.

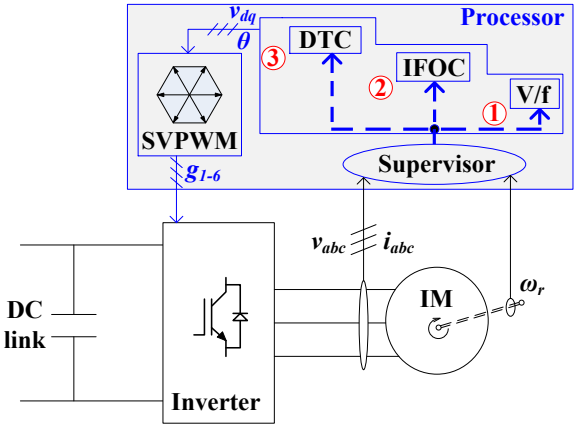

Fig. 2. System architecture of a multi-mode induction motor drive.

V/f control is essentially an open-loop control scheme and will be kept as the fundamental mode. IFOC or DTC will serve as advanced modes that the electrical drive can be switched to when superior drive performance is desired, depending on sensor availability and health. The block diagram for all three control modes is shown in Fig. 3. (a), (b), and (c), respectively [2], [3]. There is a supervisory controller within the processor that continuously monitors the system's states and determines which mode to select [4]. As far as the stability with arbitrary switching is concerned, it is necessary to require that all the subsystems be asymptotically stable. However, even when all the subsystems of a switched system are stable, such a system might fail to preserve stability under arbitrary switching but might be stabilized under restricted switching signals [6].

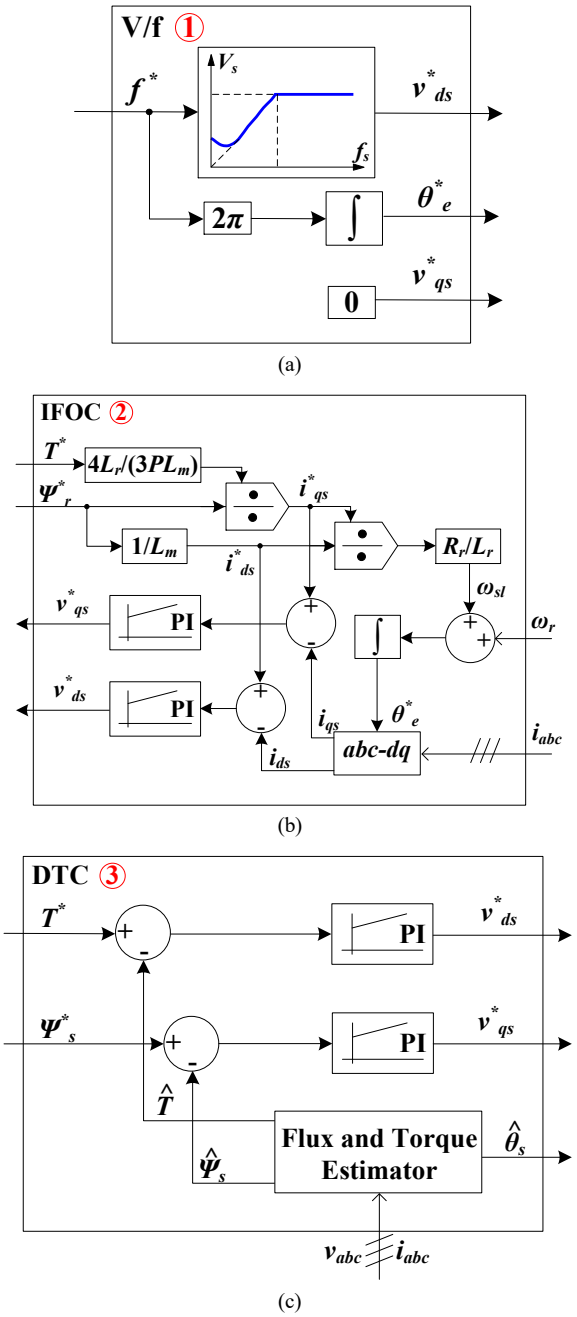

Fig. 3. Block diagram of different control strategies: (a) V/f control; (b) IFOC; (c) DTC.

Among the tools that have been developed for stability analysis of switched systems, the notion of dwell-time or average dwell-time (ADT) has played a significant role in characterization of stability conditions [7]. Unfortunately, none of the existing literatures have investigated IM drive stability under different modes in the context of switching control. In [8], the lower bounds on ADT which guarantee input to state stability (ISS) is derived within the context of stability of switched systems under slow switching. The framework proposed in [8] has provided a tool to analyze the optimal ADT that ensures stable operation of multi-mode-controlled IM drive. Before we can apply the framework to the IM drive, each subsystem's dynamics must be identified first.

The rest of the paper is organized as follows: section II discusses the lower bounds of average dwell-time for switched systems; section III presents the workflow in developing the state-space representation of motor dynamics under each control mode; section IV includes the simulation results to show the validity of the proposed state-space representation of motor dynamics under each control mode; section V concludes the paper.

II. Discussion on Average Dwell-time (ADT) in Switched Systems

Consider a class of switched linear systems given by

$$\dot{x}(t) = A_{\sigma(t)}x(t) + B_{\sigma(t)}u(t) \tag{1}$$

where $\sigma(t)$ is a piecewise constant function of time, called a switching signal, which takes its values in the finite set $S = \{1, \ldots, M\}$, and M is the number of subsystems. For a switching signal $\sigma(t)$ and each $t_2 \geq t_1 \geq 0$, let $N_\sigma(t_2, t_1)$ denote the number of discontinuities of $\sigma(t)$ in the open interval (t_1, t_2). We say that has an average dwell-time if there exist two positive numbers N_0 and τ_a such that

$$N_\sigma(t_2, t_1) \leq N_0 + (t_2 - t_1)/\tau_a, \forall t_2 \geq t_1 \geq 0 \tag{2}$$

According to [8], assume that $A_{\sigma(t)}$ are Hurwitz for all $\sigma(t)$ such that there exist positive definite symmetric matrices $M_{\sigma(t)}$, $Q_{\sigma(t)}$ and the following equation holds

$$A_\sigma^T M_\sigma + M_\sigma A_\sigma + Q_\sigma = 0 \tag{3}$$

By introducing a constant $\mu \geq 1$ such that

$$x^T M_{\sigma_1} x \leq \mu x^T M_{\sigma_2} x, \text{ for every } \sigma_1, \sigma_2 \in S \tag{4}$$

the lower bound on ADT for switched linear systems (1) can be determined as

$$\tau_a > (a/b)\ln\mu \tag{5}$$

where a and b are defined by

$$a = \max_{\sigma \in S} |\bar{\lambda}(M_\sigma)| \tag{6}$$

$$b = \min_{\sigma \in S} |\underline{\lambda}(Q_\sigma)| \tag{7}$$

and $\bar{\lambda}(.)$ and $\underline{\lambda}(.)$ denote the maximum and minimum eigenvalues respectively.

III. State-space Modeling of Induction Motor Drive Under Different Control Modes

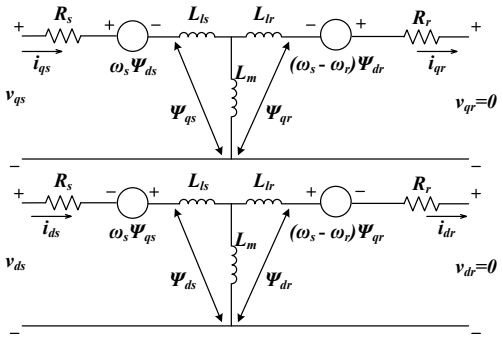

Fig. 4. Dynamic equivalent circuit of an IM in *d-q* frame [9].

In previous section, a useful framework for computing the lower bound of ADT for linear switched systems is introduced. In this section, we will be closely looking into

the problem that how the IM drive under different control modes can be modeled as linear switched systems. Fig. 4 shows the dynamic equivalent circuit of a squirrel cage induction motor in the synchronous reference frame. Such equivalent circuit can be described by a set of fifth order non-linear differential equations:

$$\begin{aligned}
\dot{\psi}_{qs} &= -\frac{R_s}{\chi_3}\psi_{qs} - \omega_s\psi_{ds} - \frac{R_s}{\chi_1}\psi_{qr} + v_{qs} \\
\dot{\psi}_{ds} &= \omega_s\psi_{qs} - \frac{R_s}{\chi_3}\psi_{ds} - \frac{R_s}{\chi_1}\psi_{dr} + v_{ds} \\
\dot{\psi}_{qr} &= -\frac{R_r}{\chi_1}\psi_{qs} - \frac{R_r}{\chi_2}\psi_{qr} - (\omega_s - \omega_r)\psi_{dr} \\
\dot{\psi}_{dr} &= -\frac{R_r}{\chi_1}\psi_{ds} + (\omega_s - \omega_r)\psi_{qr} - \frac{R_r}{\chi_2}\psi_{dr} \\
J\dot{\omega}_r &= \frac{3P}{2\chi_1}(\psi_{ds}\psi_{qr} - \psi_{qs}\psi_{dr}) - T_L \\
\chi_1 &= L_m - L_s L_r / L_m \\
\chi_2 &= L_r - L_m^2 / L_s \\
\chi_3 &= L_s - L_m^2 / L_r
\end{aligned} \tag{8}$$

where subscript d and q denote direct and quadrate axis, respectively; subscript s and r denote stator and rotor, respectively; R represents the resistance; L represents the inductance; Ψ represents the flux linkage; ω represents electrical frequency; L_m is the magnetizing inductance; P is pole pair of an IM; J and T_L are moment of inertia and applied mechanical torque on the shaft, respectively.

Based on the equivalent circuit, the state-space representations of V/f control, IFOC, and DTC are developed in the following sections. The inverter's non-linearities are ignored for simplicity. Realization of each control mode is the same as the block diagram shown in Fig. 3. Small-signal perturbation can be applied at steady-state operating point to derive a linearized model for the IM drive under different control modes.

A. Motor Dynamics Under V/f control/IFOC/DTC

For V/f control, according to Fig. 3 (a), the q-axis stator voltage v_{qs} is kept at zero, while the d-axis stator voltage v_{ds} is set proportional to ω_s. The motor dynamics under V/f control can be rewritten as:

$$\begin{aligned}
\dot{\psi}_{qs} &= -(R_s/\chi_3)\psi_{qs} - \omega_s\psi_{ds} - (R_s/\chi_1)\psi_{qr} \\
\dot{\psi}_{ds} &= \omega_s\psi_{qs} - (R_s/\chi_3)\psi_{ds} - (R_s/\chi_1)\psi_{dr} + k\omega_s \\
\dot{\psi}_{qr} &= -(R_r/\chi_1)\psi_{qs} - (R_r/\chi_2)\psi_{qr} - (\omega_s - \omega_r)\psi_{dr} \\
\dot{\psi}_{dr} &= -(R_r/\chi_1)\psi_{ds} + (\omega_s - \omega_r)\psi_{qr} - (R_r/\chi_2)\psi_{dr} \\
J\dot{\omega}_r &= (3P/2\chi_1)(\psi_{ds}\psi_{qr} - \psi_{qs}\psi_{dr}) - T_L
\end{aligned} \tag{9}$$

where $k = V_{rated}/\omega_{rated}$ defines the flux level.

Under IFOC, according to Fig. 3 (b), d-axis stator current i_{ds} is supposed to regulate the rotor flux, while q-axis stator current i_{qs} is supposed to control the electromagnetic torque. Therefore, decoupled control over rotor flux and electromagnetic torque can be achieved and the motor dynamics can be simplified as:

$$\begin{aligned}
\dot{\psi}_{dr} &= -(R_r/L_r)\psi_{dr} + (R_r L_m/L_r)i_{ds} \\
T_e &= (3P/2\chi_1)(L_m^2/L_r - L_s)\psi_{dr} i_{qs}
\end{aligned} \tag{10}$$

In DTC, according to Fig. 3 (c), the stator is to be controlled instead by the d-axis stator voltage v_{ds} and the electromagnetic torque is to be regulated by the q-axis stator voltage v_{qs} accordingly. The motor dynamics reduce to

$$\begin{aligned}
\dot{\psi}_{ds} &= -(R_s/\chi_3)\psi_{ds} - (R_s/\chi_1)\psi_{dr} + v_{ds} \\
\dot{\psi}_{dr} &= -(R_r/\chi_1)\psi_{ds} - (R_r/\chi_2)\psi_{dr} \\
T_e &= (3P/2R_s)\psi_{ds}(v_{qs} - \omega_s\psi_{ds})
\end{aligned} \tag{11}$$

B. State-state Representation Derivation of IM Drive Under V/f Control/IFOC/DTC

To derive the state-space representation of IM drive as a whole requires linearizing the motor dynamics at certain steady-state operating point and incorporating each controller's dynamics to make it a closed-loop system where applicable. Both IFOC and DTC adopt dual proportional-integral (PI) controllers to compensate for stator voltages. The transfer function of a general PI controller is:

$$\begin{aligned}
G(s) &= v/e \\
&= (v/u)(u/e) \\
&= (k_p s + k_i)(1/s)
\end{aligned} \tag{12}$$

Rewrite eq. (12) as:

$$\begin{aligned}
\dot{u} &= e \\
v &= k_p\dot{u} + k_i u \\
&= k_p e + k_i u
\end{aligned} \tag{13}$$

where s is the Laplace operator; e and v represent the input and output of a PI controller, respectively; k_p and k_i represent the proportional gain and integral gain, respectively; u is an intermediate state variable associated with the input.

According to (10, the motor dynamics under IFOC are associated with stator currents. Since the motor is usually fed by a voltage source inverter (VSI) [10], [11], the relationships between stator voltages and stator currents under IFOC are approximated as:

$$\begin{aligned}
\frac{i_{qs}}{v_{qs}} &= \frac{1}{\chi_3 s + R_s} \\
\frac{i_{ds}}{v_{ds}} &= \frac{s + 1/T_r}{\chi_3 s^2 + [R_s + \chi_3/T_r + L_m/(T_m T_r)]s + R_s/T_r}
\end{aligned} \tag{14}$$

where $T_r = L_r/R_r$, and $T_m = L_r/L_m$.

Combining (9)-(14), the state-space representation (state matrix, input matrix, state variables and inputs) of IM drive under each control mode is summarized and shown in TABLE I. Note that subscript 0 denotes the steady-state operation point where small-signal perturbation is applied, and superscript * denotes the input command. The proportional and integral gains to regulate d- and q-axis currents in IFOC are denoted as k_{p_d} and k_{i_d}, and k_{i_q} and k_{p_q}, respectively. Similarly, the proportional and integral

TABLE I. STATE-SPACE REPRESENTATION OF IM DRIVE UNDER V/F CONTROL/IFOC/DTC

V/f control

$$A_{\text{V/f}}=\begin{bmatrix} -R_s/\chi_3 & -\omega_{s0} & -R_s/\chi_1 & 0 & 0 \\ \omega_{s0} & -R_s/\chi_3 & 0 & -R_s/\chi_1 & 0 \\ -R_r/\chi_1 & 0 & -R_r/\chi_2 & \omega_{r0}-\omega_{s0} & \psi_{dr0} \\ 0 & -R_r/\chi_1 & \omega_{s0}-\omega_{r0} & -R_r/\chi_2 & -\psi_{dr0} \\ -H\psi_{dr0} & H\psi_{qr0} & H\psi_{ds0} & -H\psi_{qs0} & 0 \end{bmatrix} B_{\text{V/f}}=\begin{bmatrix} -\psi_{ds0} & 0 \\ k+\psi_{qs0} & 0 \\ -\psi_{dr0} & 0 \\ \psi_{dr0} & 0 \\ 0 & -1/J \end{bmatrix} \quad H=3P/(2J\chi_1)$$

$$x_{\text{V/f}}=[\psi_{qs} \quad \psi_{ds} \quad \psi_{qr} \quad \psi_{dr} \quad \omega_r]^{\text{T}} \; u_{\text{V/f}}=[\omega_s^* \quad T_L]^{\text{T}}$$

IFOC

$$A_{\text{IFOC}}=\begin{bmatrix} 0 & 0 & -1/T_r & -1 & 0 & 0 \\ 0 & 0 & 0 & 0 & -1 & 0 \\ 0 & 0 & 0 & 1 & 0 & 0 \\ k_{i\_d}/\chi_3 & 0 & -a_0/\chi_3-k_{p\_d}/(\chi_3 T_r) & -a_1/\chi_3-k_{p\_d}/\chi_3 & 0 & 0 \\ 0 & k_{i\_q}/\chi_3 & 0 & 0 & -R_s/\chi_3-k_{p\_q}/\chi_3 & 0 \\ 0 & 0 & L_m/T_r^2 & L_m/T_r & 0 & -1/T_r \end{bmatrix}$$

$$B_{\text{IFOC}}=\begin{bmatrix} 1/L_m & 0 \\ -WT_{e0}/\psi_{dr0}^2 & W/\psi_{dr0} \\ 0 & 0 \\ k_{p\_d}/(\chi_3 L_m) & 0 \\ -Wk_{p\_q}T_{e0}/(\chi_3\psi_{dr0}^2) & Wk_{p\_q}/(\chi_3\psi_{dr0}) \\ 0 & 0 \end{bmatrix}$$

$$a_0=R_s/T_r$$
$$a_1=R_s+\chi_3/T_r+L_m/(T_m T_r)$$
$$W=4L_r/3/P/L_m$$

$$x_{\text{IFOC}}=[u_{i\_d} \quad u_{i\_q} \quad v \quad \dot{v} \quad i_{qs} \quad \psi_{dr}]^{\text{T}} \; u_{\text{IFOC}}=[\psi_{dr}^* \quad T_e^*]^{\text{T}}$$

DTC

$$A_{\text{DTC}}=\begin{bmatrix} 0 & 0 & -1 & 0 \\ 0 & 0 & 0 & 0 \\ k_{i\_\psi} & 0 & -k_{p\_\psi}-R_s/\chi_3 & -R_s/\chi_1 \\ 0 & 0 & -R_r/\chi_1 & -R_r/\chi_2 \end{bmatrix} B_{\text{DTC}}=\begin{bmatrix} 1 & 0 \\ 0 & 0 \\ k_{p\_\psi} & 0 \\ 0 & 0 \end{bmatrix}$$

$$x_{\text{DTC}}=[u_\psi \quad u_T \quad \psi_{ds} \quad \psi_{dr}]^{\text{T}} \; u_{\text{DTC}}=[\psi_{ds}^* \quad T_e^*]^{\text{T}}$$

gains for regulations of flux and torque in DTC are denoted as k_{p_ψ} and k_{i_ψ}, and k_{i_T} and k_{p_T}, respectively.

IV. SIMULATION

A detailed model of the induction machine as well as controllers of all three control modes are simulated in MATLAB/Simulink. The induction machine's parameters are given in TABLE II. In addition, the derived state-space representations for each control mode are simulated in MATLAB/Simulink to compare their response with the detailed ones'. Fig. 5 and Fig. 6 illustrate the simulated results for IM drive under IFOC and DTC, respectively. In IFOC, the rotor flux command is set to 0.5 Wb and torque command is set to 1.5 N.m. When the drive reaches its steady state, a 10% increase in both commanded rotor flux and torque is applied. As can be seen, the derived state-space model shows similar dynamics of IM drive under IFOC as the detailed model exhibits. Same step response is tested with detailed and derived state-space model for DTC. Overall, the derived state-space model reflects the dynamics of the IM drive under each control mode as expected.

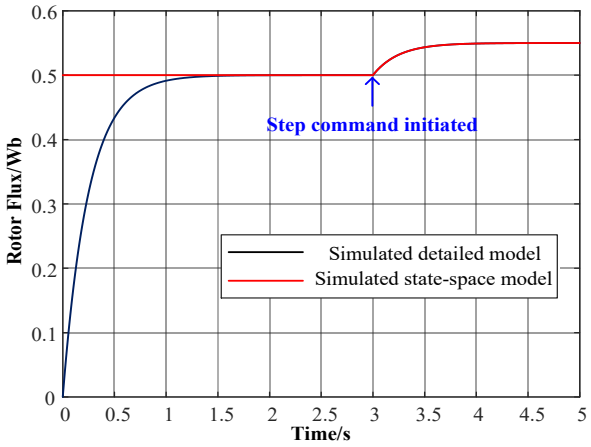

(a)

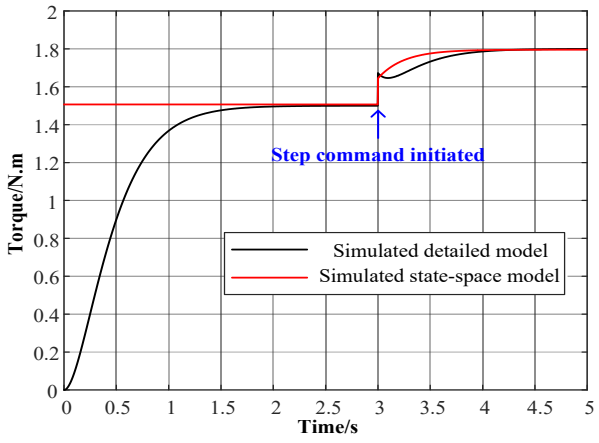

(b)

Fig. 5. Simulated step response for both detailed model and state-space model: (a) Rotor flux response under IFOC; (b) Torque response under IFOC.

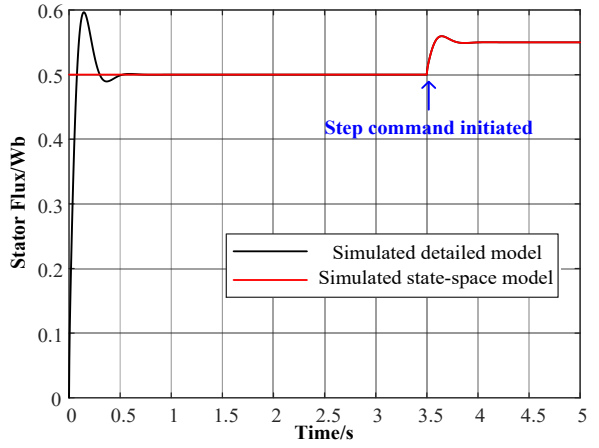

(a)

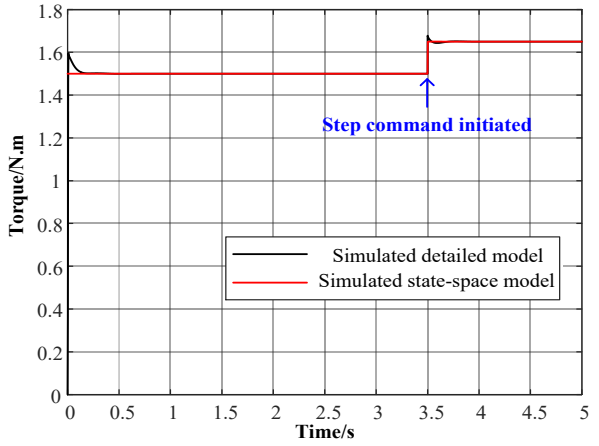

(b)

Fig. 6. Simulated step response for both detailed model and state-space model: (a) Stator flux response under DTC; (b) Torque response under DTC.

V. CONCLUSIONS

In this paper, the IM drive under different control mode is modeled from the perspective of switched systems. The concept of average dwell-time (ADT) associated with stabilized switching and its lower bound are discussed. State-space model of IM drive under different control mode is developed and validated from simulations. The proposed model provides the recipes for analysis of multi-mode-controlled IM drive under the framework of ADT in stabilizing switched systems. Further research on this topic will be reported in the future.

VI. ACKNOWLEDGEMENT

This work is financially supported by National Science Foundation under Award 1752297.

REFERENCES

[1] Z. Zhang, Y. Liu and A. M. Bazzi, "An improved high-performance open-loop V/f control method for induction machines," *2017 IEEE Applied Power Electronics Conference and Exposition (APEC)*, Tampa, FL, 2017, pp. 615-619.

[2] Z. Zhang and A. M. Bazzi, "Robust Sensorless Scalar Control of Induction Motor Drives with Torque Capability Enhancement at Low Speeds," *2019 IEEE International Electric Machines & Drives Conference (IEMDC)*, San Diego, CA, USA, 2019, pp. 1706-1710.

[3] Z. Zhang, Z.G. Liu, L.T. Zhao, L.J. Diao, "Research on AC drive test system based on vector control," in *Proceedings of the 2013 International conference on Electrical and Information Technologies for Rail Transportation (EITRT2013)*, Vol. 288, 2014, pp. 537-546.

[4] M. Stettenbenz, Y. Liu and A. Bazzi, "Smooth switching controllers for reliable induction motor drive operation after sensor failures," *2015 IEEE Applied Power Electronics Conference and Exposition (APEC)*, Charlotte, NC, 2015, PP. 2407-2411.

[5] D. Liberzon and A. S. Morse, "Basic problems in stability and design of switched systems," in *IEEE Control Systems Magazine*, vol. 19, no. 5, pp. 59-70, Oct. 1999.

[6] X. Zhao, S. Yin, H. Li and B. Niu, "Switching Stabilization for a Class of Slowly Switched Systems," in *IEEE Transactions on Automatic Control*, vol. 60, no. 1, pp. 221-226, Jan. 2015.

[7] J. P. Hespanha and A. S. Morse, "Stability of switched systems with average dwell-time," *Proceedings of the 38th IEEE Conference on Decision and Control (Cat. No.99CH36304)*, Phoenix, AZ, USA, 1999, pp. 2655-2660 vol.3.

[8] S. Liu, A. Tanwani and D. Liberzon, "Average Dwell-Time Bounds for ISS and Integral ISS of Switched Systems using Lyapunov Functions," *2020 59th IEEE Conference on Decision and Control (CDC)*, Jeju, Korea (South), 2020, pp. 6291-6296.

[9] P. C. Krause, O. Wasynczuk, S. D. Sudhoff, *Analysis of Electric Machinery and Drive Systems, Piscataway*, NJ: IEEE press, 2002.

[10] Z. Zhang, A. M. Bazzi and A. Semin, "An Active Zero-State Switch (AZS) for Commonmode Voltage Reduction in Voltage Source Inverter (VSI) Drives," *2020 IEEE Applied Power Electronics Conference and Exposition (APEC)*, New Orleans, LA, USA, 2020, pp. 711-717, doi: 10.1109/APEC39645.2020.9124003.

[11] Z. Zhang and A. M. Bazzi, "Common-mode Voltage Reduction in VSI-fed Motor Drives with An Integrated Active Zero-state Switch," in *IEEE Journal of Emerging and Selected Topics in Power Electronics*, doi: 10.1109/JESTPE.2020.3037886.